Cement and Concrete Research 40 (2010) 1609–1619

Contents lists available at ScienceDirect

Cement and Concrete Research

journal homepage: http://ees.elsevier.com/CEMCON/default.asp

Effect of microstructure and curing conditions upon the performance of a mortar added with Treated Sediment Aggregates (TSA)

F. Agostini, C.A. Davy *, F. Skoczylas, Th. Dubois

Univ Lille Nord de France, F-59000 Lille, France
ECLille, LML, BP 48, F-59650 Villeneuve d'Ascq, France
CNRS, UMR 8107, F-59650 Villeneuve d'Ascq, France

ARTICLE INFO

Article history:
Received 20 November 2009
Accepted 15 July 2010

Keywords:
Curing sediment aggregate (A)
SEM (B)
Transport properties (C)
Mechanical properties (D)

ABSTRACT

This experimental study investigates the performance of mortars added with water-saturated treated sediment aggregates (TSA), used as sand substitution (0, 33, 66 and 100% sand volume). As compared to industrial practice, two extreme curing conditions are used, either water immersion (most favorable to cement hydration), or air curing (highly deficient curing condition). Independently of curing conditions, porosity is shown to increase hugely with TSA amount, while apparent density decreases linearly with porosity increase. Nevertheless, up to 33% substitution, elastic Young's modulus, uniaxial compressive strength and apparent gas permeability are all improved as compared to reference 0%-substitution mortar. Maturity is attained from 28 to 60 curing days. The positive internal curing effect of TSA is more significant under air curing. The negative effect of brittle lightweight TSA is significant above 33% substitution. Microstructural changes have also been observed by SEM and EDS analysis, along with thermo-gravimetry analysis (TGA).

1. Introduction

Each year in France, 50 million m^3 sediments are dredged from the five biggest maritime port authorities and from the seventeen commercial ports [1]. Due to human activities, a high proportion of these sediments is polluted by both inorganic and organic matter. The Novosol™ stabilization process, patented by Solvay S.A., Belgium [2], has proven to provide an efficient immobilization of heavy metals (through a chemical treatment of phosphatation) followed by the removal of organic pollutants (through a 650 °C calcination) [3,4]. This process transforms sediments into chemically inert, light, porous and brittle aggregates. As an economically-viable alternative to disposal, giving value to these treated sediments aggregates (TSA) has been evaluated through several feasibility studies: TSA have been substituted to natural aggregates into varied building materials, such as compressed blocks [5], clay bricks [6] and mortars [7].

1.1. Specific properties of cement-based materials incorporating lightweight aggregates

Our former study [7] has underlined the lightweight (with 1.1 to 1.3 dry density) and the high water absorption capability of TSA, with absorbed amounts of ca. 45 wt.% after 24 h only. As a comparison, Bentur et al. [8] use commercially available lightweight aggregates with a water absorption of only 8.9 wt.% after 24 h. Weber et al. [9] use lightweight expanded clay aggregates with a water absorption limited to 20.2 wt.% after 24 h. High water absorption capability is generally considered as detrimental for the manufacture of cementitious materials [10]. For instance, due to higher free water amounts, open porosity increases (so that mechanical properties usually worsen [11]); drying shrinkage is enhanced. Nevertheless, Al Khaiat et al. [12] have shown experimentally that although *preliminary soaked* lightweight aggregates provide higher drying shrinkage to high-strength-concrete (HSC), water permeability is decreased, and hence, durability is enhanced. Simultaneously, early age strength is not modified notably, even under severe curing conditions.

In the same vein as [12], yet using pre-soaked TSA, our former study [7] was focused on 28 days old mortars under ideal water curing conditions. We chose a model cement-based material, i.e. a normalized mortar with a water-to-cement ratio (W/C) = 0.5. Contrarily to various studies [13–15], TSA were not used as cement substitutes but rather as sand substitutes, in proportions of 0, 33, 66 and 100% sand volume. For water-cured mortars, macroscopic properties, namely drying shrinkage, uniaxial compressive strength f_c and apparent gas permeability K were evaluated at 28 days. In particular, compressive strength f_c was found higher in presence of TSA, whatever their amount. For preliminary dried substituted mortar, gas permeability was found on the order of that of non-substituted mortar; drying

* Corresponding author. ECLille, LML, BP 48, F-59650 Villeneuve d'Ascq, France.
E-mail address: catherine.davy@ec-lille.fr (C.A. Davy).

0008-8846/$ – see front matter © 2010 Elsevier Ltd. All rights reserved.
doi:10.1016/j.cemconres.2010.07.003

shrinkage was significant, yet no major cracking was observed up to 66% substitution. These modifications in mechanical and durability performance have been explained by several mechanisms, as follows.

1.2. Performance enhancement in presence of TSA: several mechanisms may be involved

Using *carefully* pre-saturated *lightweight* aggregates has proven to have beneficial effects upon mechanical and hydraulic properties of concrete, especially in dry curing conditions [8,9,16,17]. This is due to a mechanism named *internal curing* [10,18], or *autogenous curing* [9], whereby pre-saturated lightweight aggregates constitute an internal water reservoir to help cement hydration progress more efficiently. This effect is also regarded as an efficient means to prevent micro-cracking [17], which helps reduce loss of strength under severe drying conditions [8], or for low water-to-cement ratios [9]. Yet, pre-soaking of recycled aggregates obtained from crushed building concrete has proven to have little impact on concrete mechanical properties [19–21], except for freeze–thaw resistance [19]. Instead, *semi-saturated* aggregates from crushed concrete have been recommended by Barra de Oliveira et al. [19] to maintain compressive strength, flexural strength and freeze–thaw resistance of concrete. The observed bad resistance to freeze–thaw of concrete made with dry or saturated recycled aggregates is understood as a consequence of a less dense and solid interface between cement paste and aggregate, than that with semi-saturated aggregates.

Indeed, concrete strength and durability are not only controlled by aggregate and cement paste strengths, but also by the interfacial zone between them [22,23]. In the case of lightweight aggregates, modifications of the cement paste/aggregate interface, also called interfacial transition zone (ITZ) have been observed [23,24]. In particular, the roughness of lightweight aggregate surface (as compared to the smoothness of silica sand surface) induces interlocking of cement paste on its surface [25,26]. Simultaneously, a thin porous ettringite layer of 5–10 μm is observed between cement paste and aggregate [25]. Due to its large pore size, this zone probably weakens the cement paste/aggregate bond, and hence, impacts the concrete strength. On the opposite, Elsharief et al. [27] have identified thinner and denser ITZ around lightweight aggregates, which is attributed to the internal curing effect. Despite higher aggregate porosity, this is thought to be at the origin of higher sulfate attack resistance and lower permeability than normal mortar. Penetration of cement hydration products into lightweight aggregate core has also been observed [22].

TSA are also covered with fines by 35–40 wt.%. These have a mean diameter of 11 μm, i.e. equivalent to that of usual cement powders. The addition of fine particles to cement-based materials has proven to enhance mechanical and durability performance [28], due to several possible mechanisms. In particular, fine particles provide denser packing to the cement paste [29]: this is the *filler effect*. Fine particles also reduce the *wall effect* [24,30] in the ITZ, because they fill in the ITZ, where bigger particles, due to their size, are not as numerous as within the bulk of the cement paste [29]. This densifies and strengthens the ITZ [29].

Moreover, whenever using stabilized sediments from marine origin, sodium chloride is present and still active even after treatment (it melts at 801 °C only, while the Novosol™ calcination is at ca. 650 °C). As TSA present a proportion of chlorides of ca. 2.9 at.% [31], their use should be limited to non-reinforced concrete structures. Depending on the nature of cement, it was shown in [32] that chlorides enhance cement hydration in the first 24 h, even if it is present in very small amounts (of 3% cement mass in Ref. [32]). This may contribute to the enhanced performance of TSA-substituted mortars, as observed after 28 days maturation [7].

1.3. Aims and scope of the present study

Based on the existing knowledge presented above, the actual understanding of the enhanced performance of mortars in presence of TSA has motivated the present study. The effect of curing conditions and maturation time has also been investigated.

First, the curing conditions for TSA-substituted mortars have been varied, from dry air to water immersion, both when using initially pre-soaked TSA. This will allow to distinguish between severe, dry curing conditions and ideal, water curing conditions when an infinite supply of water helps full cement hydration. This is of great practical importance, since actual curing conditions are usually in between dry air and water immersion: this study will provide lower and upper performance boundaries. We also determine macroscopic properties (Young's modulus E and compressive strength f_c) at 28, 60 and 90 days maturation. As compared to [7], open porosity measurements are refined using Mercury Intrusion Porosimetry (MIP): this provides pore size distribution of the cement paste, for both reference and 33%-substituted mortars. Secondly, in order to investigate whether fine TSA enhance cement hydration or not, thermo-gravimetry analysis (TGA) has been performed on young-age (up to 22 days old) cement pastes added with TSA limited to their fine particle content. Thirdly, in order to characterize the evolutions of ITZ in presence of TSA, scanning electron microscope (SEM) observations have been coupled to Energy Dispersive X-ray Spectroscopy (EDS) quantitative analysis of flat polished mortar surfaces. The question here is to find clues as to whether the ITZ is strengthened or weakened in presence of TSA.

2. Experimental procedure

2.1. Characterization of TSA

Sediments used in this study have been extracted from Dunkirk Authority harbor in the North of France. Raw sediments are dredged from a repair basin so that they have a high content in organic (i.e. hydrocarbon) and inorganic (i.e. heavy metals) pollutants. After treatment with the Novosol™ process (a phosphatation phase followed by 650 °C calcination), the efficiency of contamination remediation is assessed positively using leachability tests [33].

Treated sediments appear as light, porous and brittle aggregates, see Fig. 1(a) and (b). Due to the Novosol™ treatment process, TSA are sintered and rolled, so that they finally have the appearance of partly-angular and partly-rounded 0–4 mm highly-porous aggregates covered with fines. The Novosol™ treatment calcination temperature of 650 °C is high enough to decompose organic contaminants and to bring minor cohesion to the aggregates, yet it is insufficient to induce a real sintering which would close up porosity (or at least transform an open porosity in a closed one) and limit TSA brittleness. Due to the Novosol™ treatment also, no outer denser shell exists around TSA, as usually noticed with commercial artificial expanded clay aggregates [9]. Fig. 1(b), where TSA are incorporated into concrete as 100%-sand replacement, shows TSA high internal porosity and the absence of a denser shell around them (at least at the macroscopic scale).

Detailed characterization of TSA has been performed, see [7]. TSA are mainly composed of calcite, silica and of a smaller proportion (i.e. below 10% in mass) of illite, which is a non-swelling argillaceous mineral. Their main features are [7]: (1) a high water absorption capability of, on average, 45% of their initial dry mass after 24 h, (2) a high porosity, ranging from 45% for aggregates smaller than 2.5 mm to 64% for bigger aggregates, (3) a low apparent density, from 1.1 to 1.3 g/cm^3, (4) low rigidity and low resistance to crushing, since TSA are easily crushed between two fingers, and (5) a high fine content of 35 to 40% in mass, which amount is obtained after thorough washing on a 80 μm sieve. The PSD curve of TSA fines is quite narrow, although it ranges from 0.1 to 100 μm, with an average diameter of 11 μm, see [7]. No pozzolanic activity of TSA was evidenced during the feasibility study performed in our laboratory [34]. This was also confirmed by the absence of any vitreous phase in the XRD analysis of TSA, see [31].

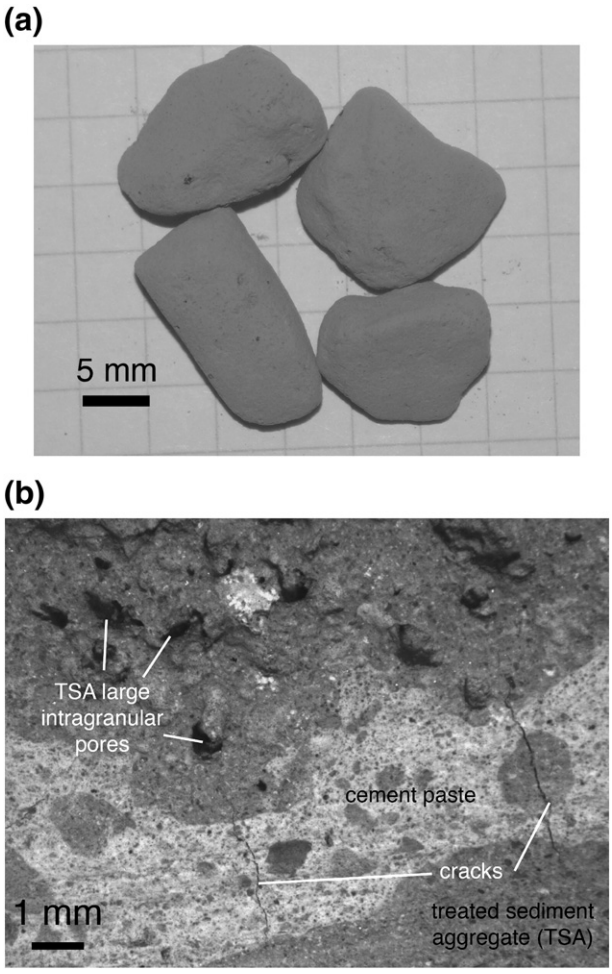

Fig. 1. (a). Photograph of TSA coated with fine particles, similar to (but bigger than) those used in substituted mortars (TSA used in mortars are less than 5 mm diameter); (b): Optical micrograph of the surface of a concrete made with 100%TSA.

2.2. Mortar design

TSA are used as a substitution material to natural sand in mortar manufacturing. Mortar is preferred to concrete as smaller and more numerous batches may be manufactured and tested. Natural sand is a 0/4 mm siliceous–calcareous river sand. Type II cement is referenced Calcia™ TechnoCem™ CEMII-B (LL-S) 32,5R. Along with a non-substituted (W/C = 0.5) normalized mortar, mortars are made by substituting sand with a given 33%, 66% or 100% volume of TSA with identical initial grain size distribution, see Table 1. Cement proportion is kept identical for all substituted mortars. Mortars are labelled RM (for reference mortar), MS33 (for 33% sand volume substitution), MS66 (66% substitution) and MS100 (100% substitution) respectively. Identical grain size distribution avoids any particular influence of the granular skeleton upon the substituted mortar properties. This is obtained by preliminary sieving. No washing of the TSA is performed.

TSA high water absorption may induce noticeable workability loss during mixing, and this is an issue in industrial practice [20]. In order to avoid this, TSA are, first, fully pre-soaked for 24 h before casting, by immersion in water amounts equal to 45% of their initial dry mass (i.e. equal to their water absorption capability). Secondly, an additional amount of mixing water is determined, so that workability, as measured by the slump test [35], is kept constant as suggested Sagoe-Crentsil et al. [21], see Table 1. As a consequence, water is added both within the TSA (during pre-soaking) and as a mortar component (during mixing). Moreover, pre-soaked TSA tend to agglomerate. Therefore, in order to properly homogenize the mix, the order of introduction of the various components into the mixer is as follows: TSA, natural river sand (if any), cement, and then water.

Having two sources of water has a consequence on the actual cement paste volume. Indeed, cement paste volume lies between two extreme cases, see Fig. 2(a) and (b). Either no pre-soaking water is released from the TSA, so that cement paste is only made of cement powder and free water added to the mix (*lower bound* case presented Fig. 2(a)). In such case, cement paste volume decreases slightly with increasing substitution amount. Or, all the pre-soaking water inside the TSA, as well as the 35 wt.% fines present at their surface, are both entirely mixed to cement powder and free water, as in Fig. 2(b) (*upper bound* case). In this instance, cement paste volume increases significantly with substitution amount. The actual cement paste volume lies between these two cases, depending on the amount of

Table 1
Formulation and slump test results for reference mortar RM and TSA-substituted mortars MS33, MS66 and MS100.

	CEM II 32.5R cement (kg)	Typical seine sand (kg)	Treated sediment aggregate (kg)	Pre-soaking water (kg)	Water added to the mix (kg)	Slump (cm)
RM	11.7	35.1	–	–	5.85	8
MS33	11.7	23.37	5.85	2.63	5.41	9
MS66	11.7	11.7	11.7	5.27	5.15	8.5
MS100	11.7	–	17.55	7.90	5.59	9

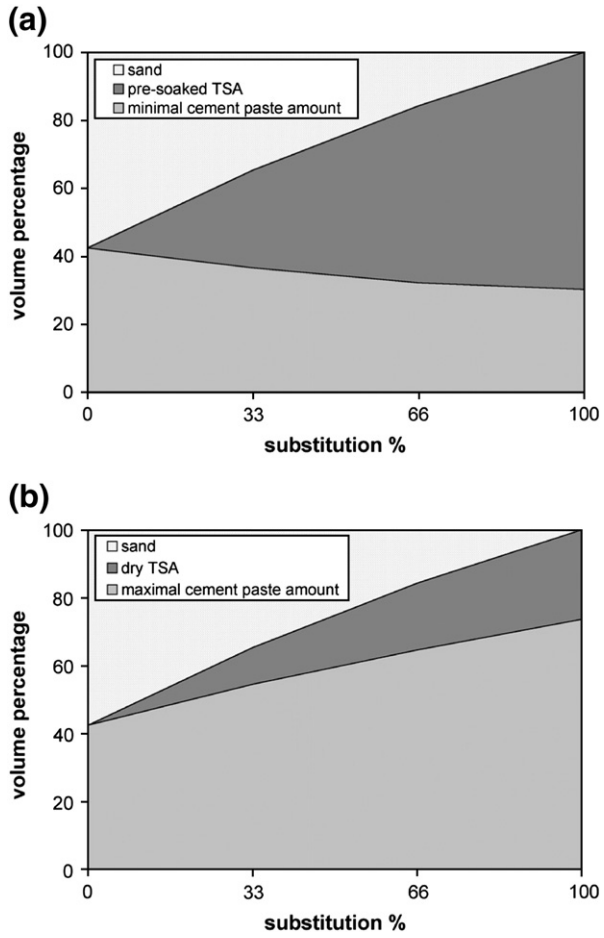

Fig. 2. Volume percentage of the main mortar constituents (sand, TSA and cement paste) as a function of substitution ratio, showing the two limit cases when (a): pre-soaking water and fine particles remain entirely within the TSA, or (b): pre-soaking water and fine particles are entirely mixed with the cement paste.

water (and fines) actually released by the TSA. For the same reason, the actual (W/C) ratio of TSA-substituted mortars is not easy to determine. Although water movement may be attributed to capillarity, from the bigger lightweight aggregate pores to the much smaller partially-dried cement paste pores [8], the water amount actually present in the cement paste cannot be assessed easily.

2.3. Sample preparation

Detailed procedure for casting and sample manufacturing is provided in former study [7]. 48 cylindrical samples (10 cm height and 36 mm diameter) and 8 prismatic samples ($4\times4\times16$ cm^3) were cast for each formulation. After 24 h for prismatic samples and an additional 24 h for cylindrical samples, un-molding was performed and samples were placed under one of two different curing conditions: (1) in a 20 °C and 60%±5 relative humidity (R.H.) controlled atmosphere, or (2) immersed in water at 20 °C±1. We have shown previously, in [28], that a 60%RH curing may be considered as a *dry* curing condition. Curing conditions were maintained for, respectively, 28, 60 or 90 days prior to mechanical and durability assessment.

2.4. Experimental procedures

Details for porosity, density, Young's modulus E, uniaxial compressive strength f_c, drying shrinkage and gas permeability K measurements are provided in [7]. In brief, porosity and apparent density were measured on cylindrical samples of 36 mm diameter and of various lengths, ranging from 1 to 3 cm, at 28 days of age only. Values presented hereafter are averages over at least two samples. For mechanical performance assessment, uniaxial compression tests were performed at a constant slow displacement rate of 2 μm/s. Being deduced from the machine crosshead displacement, Young's modulus values E are all presented as a percentage of that of the 28 days water-cured reference mortar, mainly for comparison purposes. For each formulation and curing conditions, 3 cylindrical samples (at least) were tested, after either 28, 60 or 90 days curing.

For durability assessment, drying shrinkage of prismatic samples was measured along their 16 cm length with a calibrated retractometer. Two samples of each formulation were monitored during 4 months each. Apparent gas permeability K was measured on two cylindrical samples for each formulation and curing condition, at 28, 60 and 90 days of age. Water-cured and air-cured samples were all fully dried in an oven at 105 °C until mass stabilization before permeability testing. Inert argon gas flew at an injection pressure of 1.5 MPa and the sample was subjected to a hydrostatic pressure of 4 MPa. The permeability test procedure is described further in previous studies such as [36].

Being performed later than [7], MIP results were obtained on one-year-old reference and 33% TSA-substituted mortars, corresponding to both curing conditions. Samples were of 1 cm^3-size in order to be placed inside a dedicated device (MICROMERITICS™ AutoPore IV 9500), see [28] for further details. Prior to testing, samples were oven-dried and cut to a portion limited to the cement paste.

Thermo-gravimetry analysis (TGA) was conducted on fresh cement paste, from day 1 to day 22 (and not longer due to material shortage), using a dedicated machine (Labsys by SETARAM™, France). No preliminary drying is performed. The paste is either pure (67.5 wt.% CEM I cement + 32.5 wt.% water) or added with TSA fine particles (cement + water + TSA fines). TSA fine particles are obtained after TSA washing through a 80 μm sieve. In order to be compared with previous work on high calcite fine additions [37], cement paste with a high amount of TSA fines is made with a water-to-cement ratio W/C = 0.67 and a fines-to-cement ratio F/C = 1.35. Cement pastes are reduced to ca. 60 mg ± 10 mg powder samples, and heated continuously at a rate of 5 °C/min, up to 800 °C, under an inert argon gas atmosphere. Mass loss (in mg) and heat flux (in μ V) are recorded with time. Mass loss is normalized with respect to sample cement content and expressed in percentage of cement mass (conventionally from 100% initially to lower values with heating), as follows:

$$\%m(\%\,cement\,mass) = 100^*[1 + TG(mg)^*(1 + W/C + F/C)/m_0]$$

where TG(mg) is the mass loss recorded by the machine at time t, (W/C) is the water-to-cement ratio, (F/C) is the fines-to-cement ratio and m_0 is the sample initial mass. It is generally acknowledged [38] that for temperatures ranging from ambient to 145 °C, free water and ettringite are the main responsible for mass loss, while C–S–H release chemically-bound water from 145 to 400 °C (and hence, a mass loss is recorded). Portlandite releases a water molecule between 400 and 600 °C, and calcite $CaCO_3$ releases a carbon dioxide molecule above 600 °C. Each chemical reaction corresponds to a peak of the heat flux data. Hereafter, C–S–H and portlandite amounts are compared over time between pure and TSA-fine added pastes by plotting, for both sample type, mass loss (expressed in % cement mass) between 145 and 400 °C (for C–S–H) and 400 to 600 °C (for portlandite).

Mortar microstructure was observed using a SEM instrument (HITACHI S3600N™) coupled to EDS analysis (Thermo Ultra Dry™ detector), used at a constant acceleration voltage of 15 kV. Prior to observation, air-cured one-year old mortar samples were impregnated with low viscosity epoxy resin (Epofix, Struers™). They were then polished using various discs covered with diamond wedges (ESCIL, France), and the surface was coated with a thin gold deposit (EMSCOPE SC500™ metallization instrument, by Elexience™, France). The EDS sensor allows quantitative chemical analysis with at least 1000 counts per image. For mortar, portlandite $Ca(OH)_2$ is detected as a compound devoid of silicon, containing Ca and O only. C–S–H are detected by their (C/S) ratio varying, for an ordinary Portland cement, between 1.2 and 2.3, with an average around 1.75 [39,40].

3. Results and analysis

3.1. Effect of curing conditions and age upon the macroscopic properties of mortar added with TSA

3.1.1. Porosity and apparent density

Fig. 3 presents the evolution of porosity as a function of apparent density, for reference and TSA-substituted mortars, and for both air and water curing conditions. A linear relationship is observed: density decreases with increasing TSA amount, while porosity increases, independently of curing conditions. Water curing provides continuous water supply, which should enhance hydration further than air curing, and contribute to reduce porosity and increase density [11]. Yet, no significant effect of curing conditions is observed here: the

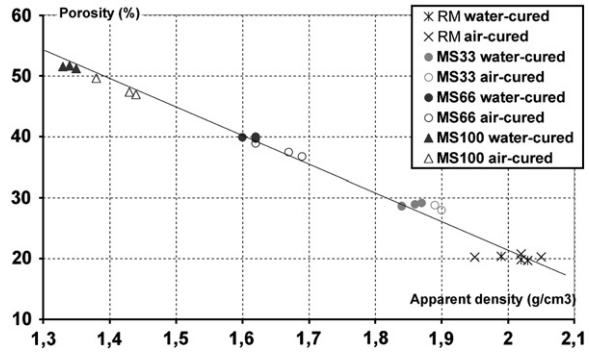

Fig. 3. Water-saturation porosity as a function of apparent density, for reference mortar RM and TSA-substituted mortars, with increasing substitution ratio, and for both curing conditions. MS33, MS66 and MS100 are TSA-substituted mortars by 33, 66 or 100% sand volume respectively.

addition of highly porous lightweight TSA is predominant as regards both porosity increase and density decrease.

Fig. 4 provides pore size distributions for reference mortar RM and 33%TSA-substituted mortar MS33, for both curing conditions, and for the cement paste portion only. MIP curves are all bimodal (with peak sizes at ca. 0.02 μm and 0.1 μm). No significant difference is noticed due to curing conditions. Pore size distributions present only a very slight, hardly significant, shift to smaller pore sizes for TSA-substituted mortars, with a higher proportion of smaller pores (of average diameter 0.02 μm) for the air-cured 33%-substituted mortar. These slightly smaller pore sizes are attributable to the presence of fine particles at the TSA surface, which get mixed into the cement paste, particularly in its bulk: this is the so-called *filler effect*. Nevertheless, our results mean that the filler effect induces a hardly significant pore size modification of the cement paste (at least down to pore sizes as measurable by MIP, i.e. above 5 nm). Therefore, it is not sufficient to explain mechanical and durability performance changes at 28 days and later.

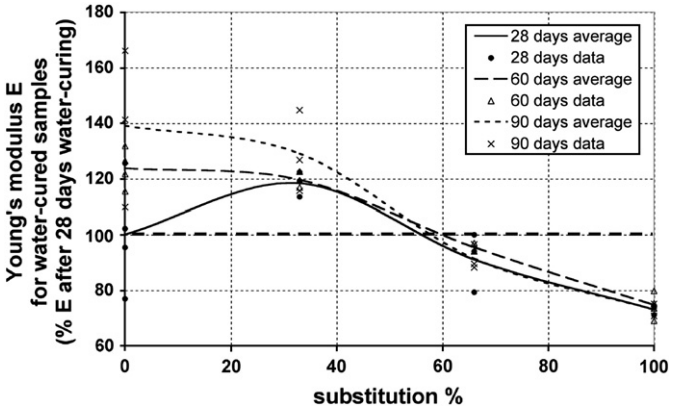

Fig. 5. Young's modulus evolution with substitution percentage for water curing conditions.

3.1.2. Mechanical performance

3.1.2.1. Young's modulus E. In Fig. 5, Young's modulus E is represented at 28, 60 and 90 days for water curing conditions, and Fig. 6 is for air curing. All values are compared to the Young's modulus at 28 days water curing and 0%-substitution (100% horizontal line).

Fig. 5 shows that Young's modulus increases with age for water-cured reference mortar only. This is attributed to continued cement hydration, thanks to extensive water supply. On the opposite, for all TSA-substituted mortars and for reference mortar under air curing conditions, maximum Young's modulus values are reached as soon as at 28 days: no further increase (or decrease) is noted at 60 or 90 days. Such early stabilization means that, as regards Young's modulus, the solid skeleton, which ensures rigidity, is not modified significantly after 28 days. For reference mortar, this is attributable to air curing, which hinders further cement hydration after 28 days. For TSA-substituted mortars, it means that the internal curing effect is not sufficient to bring significant modifications to the solid skeleton rigidity after 28 days. Another interpretation is that, in presence of TSA, cement hydration is accelerated during the first 28 days, so that no more increase may be obtained later. Such interpretation is unvalidated in Section 3.2.1.

Rather, mortar rigidity is the addition of (1) the high rigidity of sand aggregates (when they are present), of (2) the much lower rigidities of cement paste and TSA, and also of (3) *varied* micro-cracks contribution [11]. Indeed, when present, generally at the cement paste/aggregate interface, micro-cracks allow local sliding under load, which reduces rigidity [11]. In presence of lightweight TSA, the rigidity of cement paste and TSA has a better compatibility than between cement paste and sand grains, so that micro-crack amount is lower than for reference mortar [41]. The internal curing effect also helps reduce micro-cracking [17]. The reduction of the wall effect in presence of TSA fines may have a contribution too [29]. In presence of TSA, smaller amounts of micro-cracks induce a rigidity increase, which is counterbalanced by TSA high deformability. This is consistent with the stress–strain curves: these are linear up to 90% of f_c in presence of up to 33% TSA, whereas the stress–strain curves display much more ductility for reference and 66 to 100%-TSA mortars.

Under water curing conditions, Young's modulus at 28 days remains stable up to 33% substitution: the positive effect of smaller amounts of cracking in presence of TSA predominates. For higher substitution ratios than 33%, E decreases down to values lower than for reference mortar: this is attributed to greater amounts of highly deformable TSA, which predominate over smaller micro-cracking amounts.

Under air curing, Young's modulus at 28 days is lower than that of water-cured reference mortar (RM), except at 33% substitution where it is equivalent to water-cured RM. Here, the contribution of the internal curing effect is more obvious than under water curing: water present inside the TSA provides rigidity enhancement, very possibly by reducing micro-cracking at the ITZ between cement paste and TSA. At 66 and 100% substitution, the negative contribution of highly deformable TSA prevails upon internal curing.

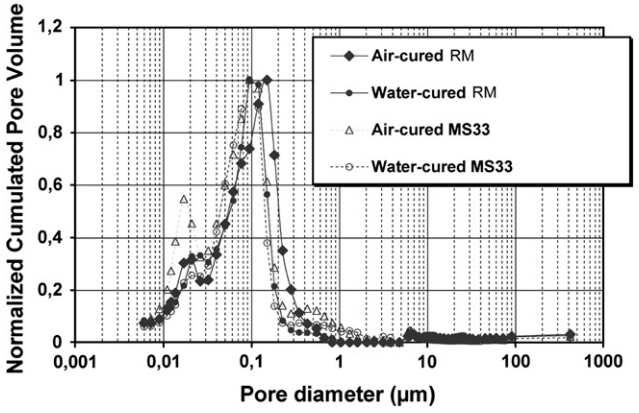

Fig. 4. Normalized pore size distribution for reference and 33% TSA-substituted mortars as measured by MIP.

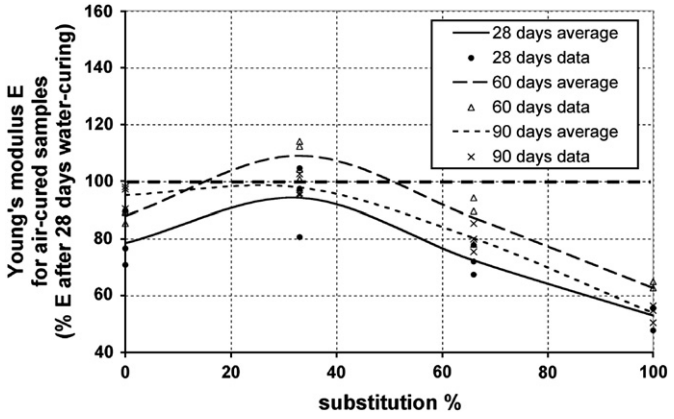

Fig. 6. Young's modulus evolution with substitution percentage for air curing conditions.

3.1.2.2. Uniaxial compressive strength f_c. Figs. 7 and 8 provide f_c with increasing substitution ratio and mortar age for, respectively, water curing and air curing conditions.

The effect of age is significant only under water curing, for reference and 33%-substituted mortars: f_c increases up to 60 days. As A. M. Neville [11] recalls, the progression of micro-cracking also dominates the strength of cement-based materials: the lower the micro-crack amount, the greater the strength. While maturation is complete at 28 days as regards Young's modulus (and rigidity) for RM and 33%-substituted mortars, further strength enhancement is obtained up to 60 days. This may mean that a portion of micro-cracks existing at 28 days gets filled with hydration products even after that time, so that micro-crack amount is lower at 60 days than at 28 days, and, hence, f_c is higher at 60 days than at 28, without significant effect upon rigidity.

For water-cured mortars at full maturation, f_c is greater or equivalent to reference mortar value with a maximum reached at 33% substitution. Such good performance is attributed to smaller micro-crack amounts. Yet, this positive effect is counterbalanced by TSA high brittleness. Indeed, the crushing of TSA is bound to be greater above 33% substitution, so that f_c decreases down to values equivalent to reference mortar.

As expected, under air curing, compressive strength is lower rather than under water curing, whatever the substitution ratio. Nevertheless, the internal curing effect has several positive consequences. For 33%-TSA substituted mortar under air curing, f_c reaches a value equivalent to that of RM under water curing. In presence of TSA, the difference between air-curing and water-curing strength is lower than for reference mortar. This also means that, for air-cured material, the strength improvement is greater than under water curing. In particular, the increase in strength amounts to 42% of RM value at 33% substitution and 28 days for air-cured mortar, and to only 17% of RM value for water curing. Under air curing, whatever the substitution ratio, TSA presence induces a higher f_c than for reference mortar.

3.1.3. Mortar durability

Durability is assessed by using both drying shrinkage and apparent gas permeability measurements.

3.1.3.1. Drying shrinkage. Drying deformations are of shrinkage for air-cured mortars after 28 or 120 days [7], while these consist of expansion under water cure after 28 days, see Table 2. No value at 120 days could be recorded for water-cured samples, due to technical problems (end studs got covered with calcite). As Bentur et al. [8] recall, the difference in shrinkage behavior is due to continuing hydration under water cure, so that mortar keeps expanding, whereas it shrinks when water supply is limited. Here, drying shrinkage keeps increasing with substitution ratio. Values for substituted mortars are 9.6 times higher than for reference mortar at 100% substitution and 28 days, while shrinkage values are 8 times higher than reference value at 100% substitution and 120 days. Therefore, the internal curing effect seems insufficient to provide full mortar protection: micro-cracking is bound to occur due to drying, depending on the sample size. Nevertheless, up to 66% substitution, no cracking was observed visually, either on cylindrical samples (10 cm height and 36 mm diameter) or on prismatic samples ($4\times4\times16$ cm^3).

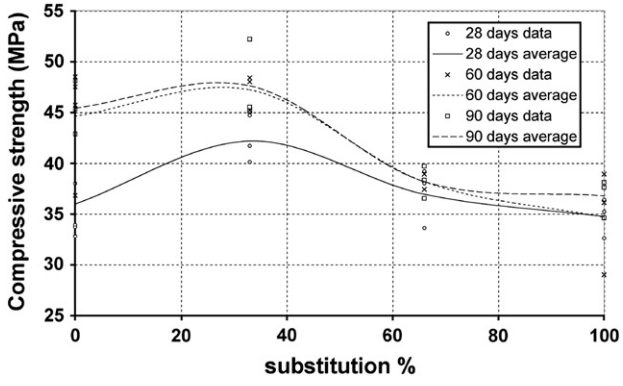

Fig. 7. Effect of cement maturation upon uniaxial compressive strength: results for water-cured samples after 28, 60 and 90 days curing.

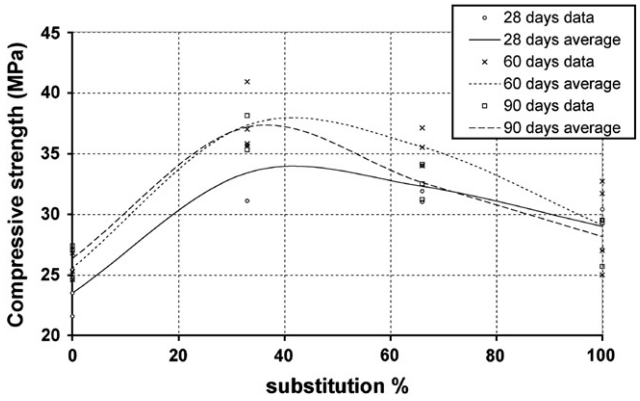

Fig. 8. Effect of cement maturation upon uniaxial compressive strength: results for air-cured samples after 28, 60 and 90 days curing.

3.1.3.2. Gas permeability K. Permeability is generally agreed to be a good durability indicator for cement-based materials [41]. Fig. 9 shows gas permeability results as a function of substitution ratio, curing conditions and age, for preliminary oven-dried samples. First, it is observed that curing duration (28, 60 or 90 days) is not strongly influential on gas permeability: gas passages are fully formed as soon as at 28 days of age, and very possibly earlier. Gas pathways consist of (1) the connected pore network of the cement paste, (2) TSA internal pores, and (3) micro-cracked interfaces between cement paste and aggregates. These are more numerous between sand grains and cement paste rather than between TSA and cement paste, due to a better ITZ in the latter case, see also Section 3.2. TSA internal pores have a limited participation in the gas flow. Indeed, after water curing, permeability K does not change of order of magnitude (10^{-17} m^2) up to 100% substitution; K becomes three to four times higher than RM above 33% substitution only.

Permeability of water-cured mortar is sensibly lower than that of air cured mortar, whether it is TSA-substituted or not. This is attributed to the protection, provided by water, against drying shrinkage, which induces smaller micro-cracking amount than under air curing. This interpretation is consistent with higher strength f_c, which was observed for water-cured mortars as compared to air-cured ones, see Section 3.1.2. above. Under water curing conditions, permeability remains unchanged up to 33% substitution. Although multiplied by 3 (to 4) for higher substitution ratios, permeability remains very low, with values of ca. 3.7×10^{-17} m^2. Again, this is consistent with the fact that f_c remains

Table 2
Drying shrinkage (or expansion) measured on prismatic $4\times4\times16$ cm^3 samples after 28 days water-curing or 28 and 120 days air-curing.

	RM	MS33	MS66	MS100
Expansion of water-cured samples after 28 days (μm/m)	+78	+208	+235	+489
Drying shrinkage of air-cured samples after 28 days (μm/m)	−430	−1200	−2480	−4130
Drying shrinkage of air-cured samples after 120 days (μm/m)	−600	−1440	−2950	−4790

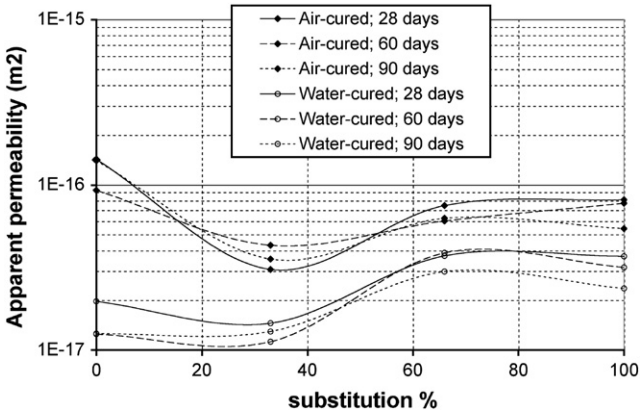

Fig. 9. Apparent permeability of air- and water-cured samples after 28, 60 and 90 days curing.

higher or equivalent to RM value whatever the substitution ratio, in relation with a smaller micro-cracking amount.

For air-cured reference mortar, the apparent gas permeability is on average 1.4×10^{-16} m^2. Noticeable scatter of this result is observed (from 1.73×10^{-16} to 9.52×10^{-17} m^2). This is attributed to the measurement protocol, to the sampling method (which consists in molding small mortar samples and not coring samples from a bigger beam), to the intrinsic variability of cementitious materials micro-structure, and to probable micro-cracks presence, enhanced by dry curing, which may affect samples randomly. As for substituted mortar, permeability of air-cured material is noticeably lower than reference mortar RM: this is attributed to the internal curing effect. The 33% substituted mortar goes down to 3×10^{-17} m^2, i.e. its permeability is divided by 5 as compared to RM. Permeability is divided by about 2 for 66 and 100% substitution. This confirms an optimal substitution ratio of 33% sand volume (as compared to 66 and 100%), as observed in terms of uniaxial compressive strength. Low permeability of air-cured substituted mortars also means that no extensive micro-cracking has occurred within the material, despite high drying shrinkage values, see Table 2: durability is preserved in presence of TSA, so that possible ingress of aggressive agents remains limited.

Finally, the permeability ratio between water curing and air curing K(water)/K(air) is of 7 for reference mortar, and it decreases down to about 3 for TSA-substituted mortars. Again, TSA presence limits performance loss under deficient curing, very possibly thanks to the internal curing effect.

3.2. Microstructure changes due to the presence of TSA

3.2.1. Is cement hydration accelerated in presence of TSA?

In presence of lightweight aggregates, one reason invoked by A. M. Neville [11] for the acceleration of cement setting is the better thermal insulation of substituted mortar thanks to increased porosity. This induces higher temperature in the sample core, resulting in faster cement hydration. Nevertheless, evaluating the thermal insulation capability of TSA, as compared to that of sand grains, was not undertaken here. Instead, we have assessed whether adding TSA fines to cement paste helps accelerate its hydration.

TGA results are provided in Fig. 10(a) for C–S–H decomposition amount and in Fig. 10(b) for portlandite decomposition amount, as a function of cement paste age. We have only tested reconstituted cement pastes: observed effects relate more to the bulk cement paste in presence of TSA fines (or not), than to the ITZ. Results are limited to 22 days due to material shortage, and also because acceleration effects should be noticed as early as within the first 24 h, see [32].

First, C–S–H decomposition is slightly more important in the first few hydration days in TSA-substituted paste rather than in pure paste. For instance, after 4 days hydration, pure cement paste loses 8% ±0.8

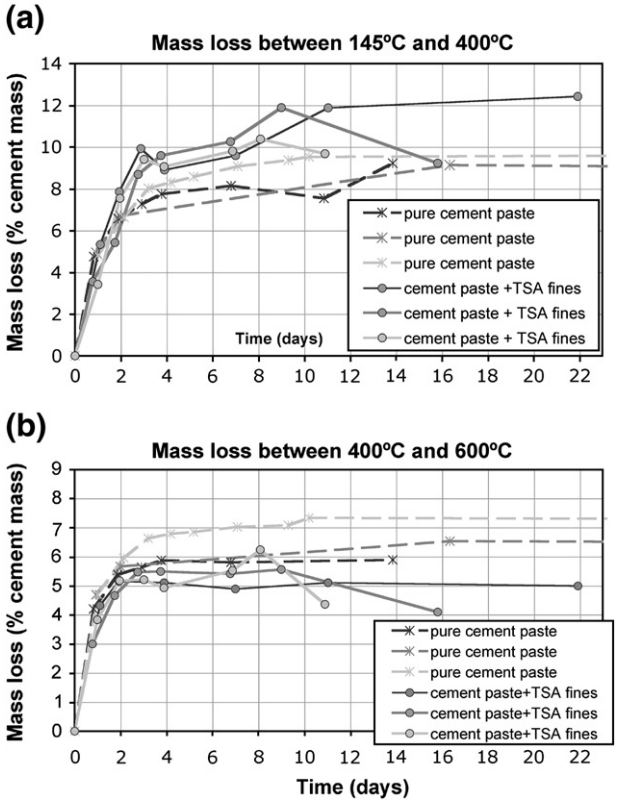

Fig. 10. TGA analysis results for (a) C–S–H (sample mass loss ranges from 145 to 400 °C) and (b) Portlandite $Ca(OH)_2$ (sample mass loss ranges from 400 to 60 °C): comparison between reference cement paste and cement paste added with 45 wt.% fine TS particles.

mass corresponding to C–S–H decomposition, whereas TSA-added paste loses by 9.3% ±0.5 mass. This means that C–S–H formation is slightly accelerated in presence of TSA fine particles, possibly because these act as additional nucleation sites for C–S–H, or rather, due to the presence of 2.9 at.% of chlorides. Nevertheless, this difference is rather slight, and it becomes insignificant after 10 days hydration. Indeed, from 10 days onwards, mass loss corresponding to C–S–H decomposition reaches a value of ca. 10%, both for cement pastes added with TSA fines and for pure cement pastes, see Fig. 10(a). Simultaneously, mass loss corresponding to portlandite decomposition is similar for TSA fine-added cement pastes and for pure cement pastes, with a maximum difference of less than 1% whatever the age. In brief, the presence of TSA fines does not induce any significant difference in phase composition after 10 days hydration, the difference before 10 days being very slight. It is concluded that the presence of TSA fines does not enhance significantly cement hydration on the medium and long terms.

3.2.2. How is the ITZ modified in presence of TSA?

After sample preparation, see Section 2.4., and as suggested by [42], the quality of surface polishing has been assessed on a 33% substituted mortar sample by SE imaging, see Fig. 11(a), and also by BSE observation, using both compositional and topographic images, see Fig. 11(b) and (c). These three images of the same sample location attest of an acceptably limited relief as exemplified in [42], despite a strong hardness difference between sand grains (in dark grey on Fig. 11(b)) and cement paste (with different grey levels in Fig. 11(b)), at a magnification comparable to those used in the following.

Then reference mortar has been observed, see Fig. 12. This provides several expected features. Coupled EDS analysis shows that uniform dark grey zones are silica grains, surrounded by medium to light grey cement paste. Using EDS analysis, we have evidenced two portlandite deposits (these are circled) located at the interface between sand grain

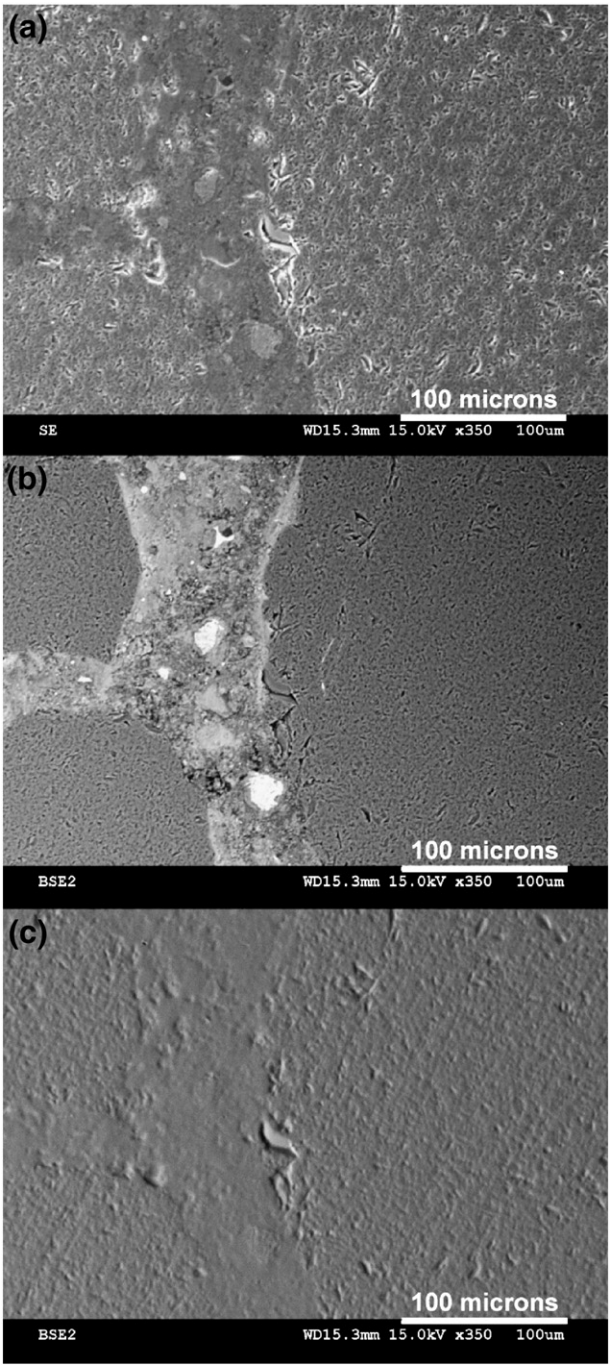

Fig. 11. The surface flatness quality is observed by (a): SE imaging, (b) compositional BSE imaging, and (c): topographic BSE imaging at the same location, as proposed in [42]. Example of a 33%-TSA substituted mortar.

and cement paste. These are present all over the sample surface, still at the sand grain/cement paste interface, but they never surround it entirely. Such portlandite deposits induce a weakening of the sand grain/cement paste interface [24]. Capillary pores correspond to the darkest (almost black) grey level, which is spanned over very small surfaces distributed all over the cement paste.

Preliminary optical microscope observations have also been performed on an air-cured concrete incorporating 100% TSA as aggregates, see Fig. 1 (b). The TSA/cement paste interface does not display noticeable cracking; rather, cracks pass perpendicularly to the interface and right through sediment aggregates (see small TSA on the right of the micrograph). This is confirmed by SEM observations of a

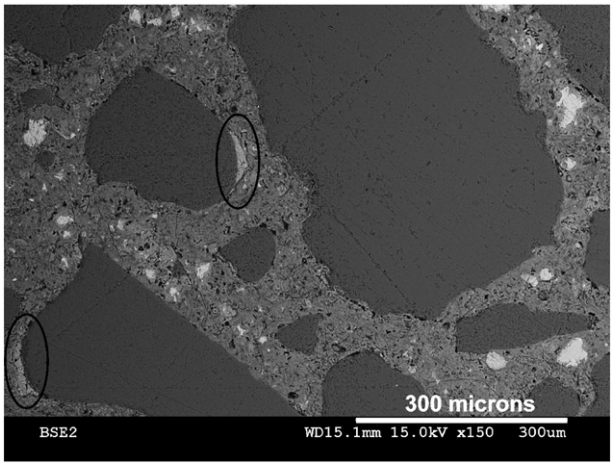

Fig. 12. SEM image (using BSE detector) of air-cured reference mortar RM. EDS analysis shows that darker grey zones are silica grains, surrounded by medium grey cement paste. Two portlandite deposits (circled) have also been located at the interface between sand grain and cement paste. The darkest grey level corresponds to capillary pores.

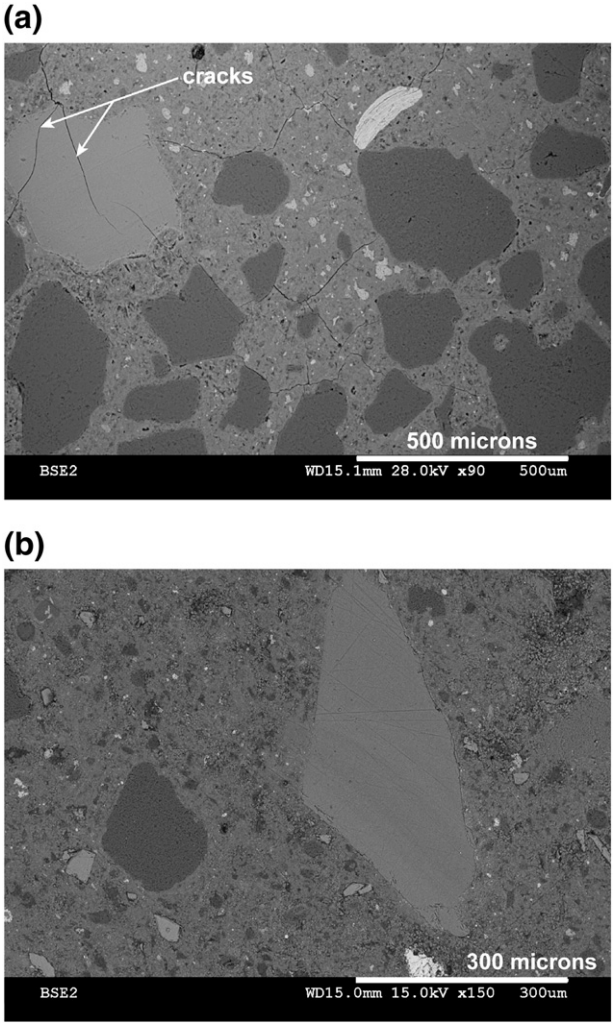

Fig. 13. SEM image of (a): a 33%-TSA substituted mortar (using the BSE detector) showing various sand aggregates (in dark grey) and a TSA aggregate (in light grey) surrounded by cement paste; (b) a 100%-substituted mortar with two TSA aggregates (dark grey on the left, light grey on the right).

33% TSA-substituted mortar, see Fig. 13(a). Various sand aggregates (in dark grey) are observed, and a TSA aggregate (in light grey, top left of image) is gone right through by several micro-cracks. This is not observed with silica sand aggregates, because in their case, micro-cracks pass preferably at the interface rather than through the aggregate. In both microstructures displayed on Figs. 1(b) and 13(a), micro-crack origin may be either drying shrinkage or sample preparation procedure. Crack paths going right through TSA is typical of an interface stronger than the TSA themselves, whereas with sand aggregates, the ITZ is weaker than the aggregate.

TSA presence has been observed on 100%-substituted mortar, see Fig. 13(b). Different grey levels may correspond to the TSA, depending on their exact chemical composition. In substituted mortars, two types of interfaces between TSA and cement paste have been observed qualitatively, see Figs. 13(a) and (b), 14 and 15. In the first case, a neat, distinct interface between the TSA surface and that of the cement paste is observed, see in particular Fig. 14: although the TSA surface is rather porous on a small width (less than 10 μm), no interlocking between cement paste and TSA is clearly visible at the magnifying scale used. In the second case, an interfacial layer, which is neither the cement paste, nor the TSA, is observed, see Fig. 15: the TSA is entirely surrounded by a very thin rim (less than 1 μm) of greater density than both TSA and cement paste, due to its lighter grey color. At the TSA bottom left corner, the interfacial layer becomes thicker, by ca. 2 μm, and it is partially spread over both TSA and cement paste. EDS analysis of this zone is provided in Table 3(a) and (b). First, the (C/S) ratio shows that only surfaces 8 and 9, located in the cement paste, correspond to C–S–H, with values in the acceptable interval of 1.2 to 2.3 [39,40]. Points 6 and 7 are within the TSA grain, which has a very varied composition, with oxygen, sodium, traces of magnesium, aluminium, silicon, potassium, traces of calcium, titanium and iron. Points 1 to 5 relate to the ITZ between TSA and cement paste: like TSA, its stoichiometry is complex, with atoms similar to those of the TSA, yet in different proportions. The ITZ is not C–S–H (see (C/S) ratio) or ettringite, due to the absence of sulphur.

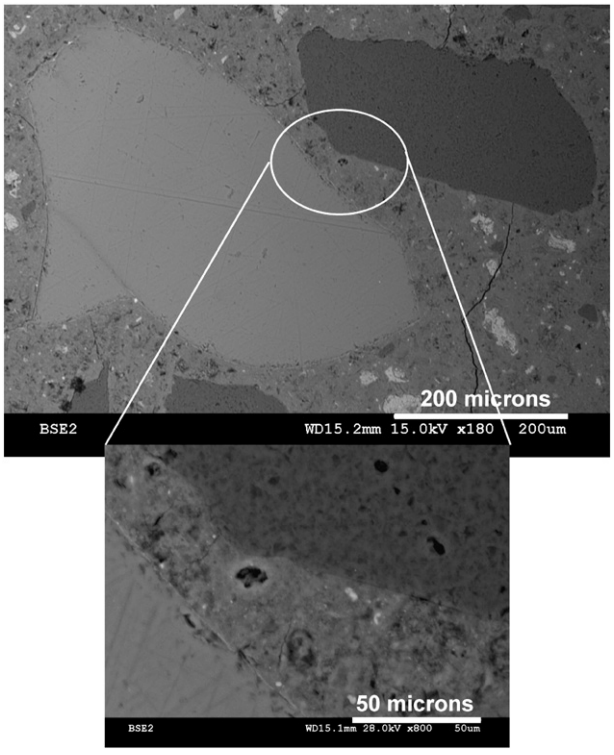

Fig. 14. BSE image of a TSA (light grey) present in a 33% substituted mortar. A sand grain is also observed (dark grey, top right corner). The interface between TSA (or sand grain) and cement paste is zoomed in.

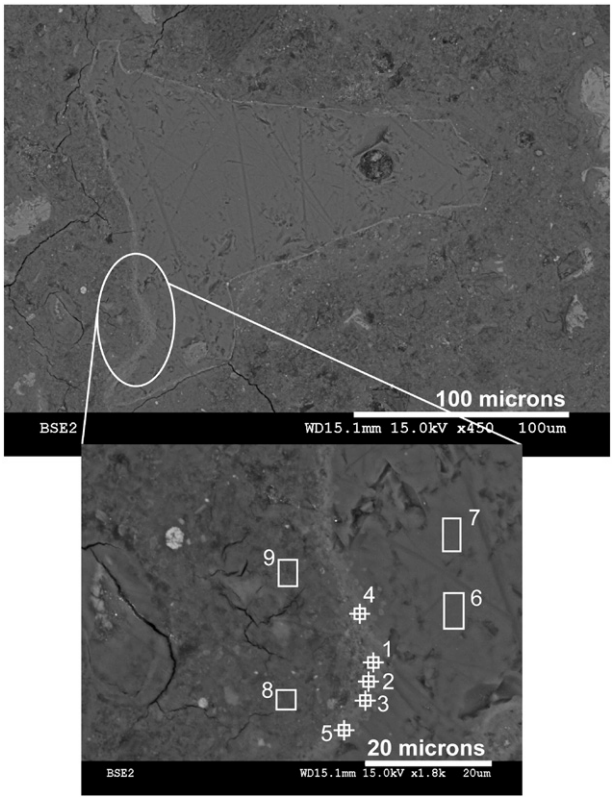

Fig. 15. BSE image of a TSA present in a 33% substituted mortar. The wider interface between TSA and cement paste (bottom left) is zoomed in and identified by EDS analysis.

In presence of TSA, the interface between sand grain and cement paste is also modified significantly. First, on the whole 4 cm^2 surface of the 33% substituted mortar sample, no more portlandite deposit is observed at the sand grain/cement paste interface: the weakening effect of these deposits is cancelled in presence of TSA. Secondly, the sand grain/cement paste interface is partially surrounded by a densified

Table 3
(a) and (b) EDS analysis results (expressed in wt.%) for the points described Fig. 15. The (C/S) ratio is also provided.

(a)	C	O	Na	Mg	Al	Si
Point 1	–	32.86	2.07	1.38	11.78	22.94
Point 2	–	28.15	2.10	1.36	12.82	24.70
Point 3	–	29.92	2.49	1.28	13.17	24.78
Point 4	–	29.76	2.21	1.38	12.33	23.84
Point 5	14.09	28.14	1.62	0.77	10.44	20.49
Point 6	14.43	36.29	2.27	0.77	11.38	21.36
Point 7	–	36.22	3.00	1.19	14.77	27.44
Point 8	9.16	40.59	–	–	1.60	10.65
Point 9	9.82	39.87	0.79	0.62	1.72	8.99

(b)	Cl	K	Ca	Ti	Fe	(C/S)
Point 1	–	3.29	9.54	2.96	13.19	0.46
Point 2	–	4.30	7.97	3.45	15.17	0.40
Point 3	–	5.31	6.10	3.07	13.88	0.36
Point 4	0.31	3.86	9.06	3.13	14.11	0.43
Point 5	–	4.45	5.82	2.77	11.40	0.39
Point 6	–	4.27	1.20	3.02	5.01	0.29
Point 7	–	4.78	1.61	3.78	7.20	0.26
Point 8	–	–	37.35	–	–	1.35
Point 9	–	0.55	36.33	–	–	1.40

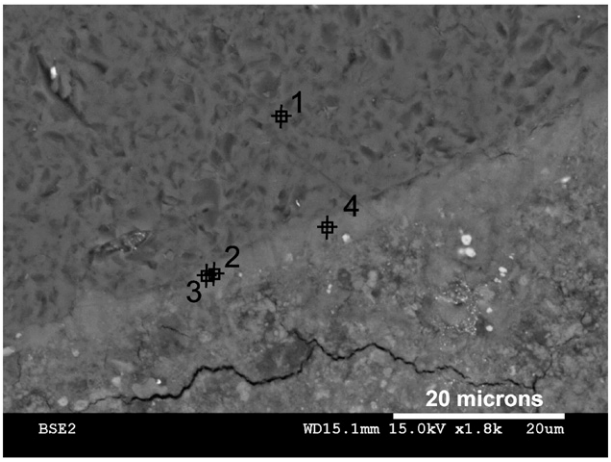

Fig. 16. SEM image (using BSE detector) of air-cured 33% TSA-added mortar: the sand aggregate is in dark grey (top left) and the cement paste is in lighter grey (bottom right). The location of EDS analysis points is also labelled, from 1 to 4 (see Table 3 for corresponding quantitative results).

interfacial layer of no more than 2 to 5 μm thickness, which is not observed on reference mortar RM, see Fig. 16. This interfacial zone is denser than its surrounding sand grain and cement paste due to its lighter grey level. It is observed at several locations all over the 33% substituted mortar sample surface. EDS analysis of three representative points taken within this interfacial zone is provided in Table 3. Comparable quantitative results have been obtained on several other similar interfacial zones. In Table 4, Point 1 is within silica SiO_2 grain, while Points 2 and 3 clearly correspond to a typical C–S–H phase. For Point 4, the (C/S) ratio is rather too low to correspond to a typical C–S–H, and the presence of a small amount of Ni (and traces of Mg too) indicates a more complex stoichiometry. Al and S elements are not present in sufficient amount to indicate ettringite presence, as was observed by [25]. It is concluded that the presence of TSA induces a partial, thin and dense C–S–H layer at the sand/cement paste interface. Denser ITZ was shown to contribute to higher strength [22], and lower permeability [24], as observed here, see Section 3.1.

4. Conclusion

Following previous work [7], the substitution of high quantities of natural sand by TSA in mortar is not only technically feasible, but it allows to obtain mortar with enhanced mechanical and hydraulic performance, especially in severe, dry, curing conditions. This is attributed to lower micro-crack amount at the interface between aggregate/cement paste in presence of TSA; it is counterbalanced by TSA high deformability and brittleness. Lower micro-crack amount is the consequence of TSA internal curing, better compatibility between TSA aggregate and cement paste, and water curing. The reduction of the wall effect thanks to TSA fines may also have a contribution. Our main results are:

- Apparent density decreases linearly with open porosity increase, solely due to the increasing addition of lightweight TSA: no effect of mortar age is recorded. Similar pore size distributions are obtained by MIP for the cement paste of RM and 33% TSA-added mortar: no significant filler effect is evidenced.
- In presence of TSA, elastic Young's modulus E reaches a maximum as early as at 28 days maturation. For water curing, E remains stable up to 33% substitution, thanks to lower micro-cracking amount at the aggregate/cement paste interface. For air curing, E is enhanced up to 33% substitution so as to reach water cured RM value, mainly due to the internal curing effect, which also reduces micro-cracking. Above 33% substitution, whatever the curing conditions, E decreases regularly with TSA amount, due to the predominance of TSA high deformability.
- Uniaxial compressive strength f_c reaches a maximum at 60 days maturation for water cured mortars and substitution ratios up to 33%, whereas maturation is attained at 28 days above 33% substitution or after air curing. After water curing, f_c is higher or equivalent to that of reference mortar RM. This is due to lower micro-cracking amount at the interface between aggregate/cement paste when TSA are present. After air curing, f_c is greater in presence of TSA, so as to reach water cured RM value at 33% substitution. Again, this is mainly attributed to the internal curing effect provided by initially saturated TSA. Whatever the curing conditions, the decrease in f_c above 33% substitution is attributed to the greater contribution of TSA brittleness.
- In air curing conditions, drying shrinkage is hugely enhanced by TSA presence (it is multiplied by 2.4 at 120 days for 33% substitution ratio), whereas increased expansion is obtained under water curing (it is multiplied by 2.6 at 28 days for 33% substitution). Although this is usually detrimental to mortar durability, apparent gas permeability K is lowered by TSA presence up to 33% substitution, whatever the curing conditions. This result is attributed to lower micro-cracking. Under air curing conditions, K remains lower than RM for all substitution ratios, whatever the age considered up to 90 days. After water curing, K is multiplied by 3 (to 4) above 33% substitution, but it remains on the same order of magnitude (10^{-17} m^2).
- TGA has shown a ca. 1% increase in C–S–H amount at early age (less than 10 days) for a TSA fine-added cement paste, as compared to pure cement paste. This is attributed to a slightly accelerating effect of cement hydration, due to fine particles of TSA. Yet, after 10 days hydration, no more difference is noted between TSA-added and pure cement pastes.
- Finally, SEM observations show the presence of weakening portlandite at the sand grain/cement paste interface in RM. Portlandite deposits were not observed on 33% substituted mortar. Instead, for 33% substitution, a ca. 2 to 5 μm thick and dense C–S–H layer is observed at varied locations of the sand grain/cement paste interface. Between TSA and cement paste, the ITZ is either neat at the observed scale, or it presents a distinct and very thin (less than 1 μm), denser, interfacial zone. This zone may partially thicken and get spread over cement paste and TSA. Both types of interfaces (between sand grain/cement paste or TSA/cement paste) are generally densified, which means that they are strengthened. Indeed, in all observations, micro-cracks propagate from the cement paste through the TSA, and not through their interface. This is thought to explain the improvements in E and f_c, and the lower permeability K.

Table 4
EDS analysis results (expressed in wt.%) for the points described Fig. 16. The (C/S) ratio is also provided.

	C	O	Mg	Al	Si	S	Ca	Ni	(C/S)
Point 1	20.56	41.98			37.46				–
Point 2	9.81	42.83			3.85		43.51		1.78
Point 3	10.28	36.74		0.37	9.65	0.97	41.99		1.59
Point 4	12.70	39.46	0.29		12.81		33.71	1.03	1.19

Acknowledgments

The authors wish to acknowledge financial support of Solvay S.A., Belgium (Mr. G. Depelsenaire). We are also grateful to Ms. Victoria Gea Lopez for her contribution to process TGA results, and to Mr. Jean-Yves Dauphin for his expertise in SEM observations and EDS analysis.

References

[1] C. Alzieu, in: Ifremer Plouzanée (Ed.), Dragages et Environnement Marin : état des connaissances (dredging and marine environment: a state of the art), 1999, France, ISBN 2-84433-1999;014-2;223.

[2] S.A. Solvay, Belgium, Contaminated sediment stabilization process, European Patent EP1341728 (19/04/2002) and French Patent No.: FR2815338 (17/10/2000, 2000 and 2002.

[3] Z. Lafhaj, M. Samara, L. Boucard, F. Agostini, F. Skoczylas, Polluted River Sediments: Characterization, Treatment and Valorization, Proceedings of the First Euro Mediterranean in Advances on Geomaterials and Structures, Hammamet, Tunisia, May 2006.

[4] S. Kribi, A. Nzihou, P. Sharrock, G. Depelsenaire, Stabilization of Heavy Metals from Sediments Tailoring of Residue Properties, Proceedings of the Third International Conference on Remediation of Contaminated Sediments, Battelle Press, New Orleans, Louisiana, USA, January 2005, ISBN: 1-57477-150-7.

[5] L. Boucard, Z. Lafhaj, F. Skoczylas, River Sediments Contaminated by Heavy Metals and Organic Compounds: Characterisation, Treatment and Valorization, Proceedings of the Conference on the Use of Recycled Materials in Buildings and Structures, RILEM, Barcelona, Spain, November 2004, pp. 807–813.

[6] Z. Lafhaj, M. Samara, F. Agostini, L. Boucard, F. Skoczylas, G. Depelsenaire, Polluted river sediments from the North region of France: Treatment with Novosol® process and valorization in clay bricks, Constr. Build. Mater. 22 (5) (May 2008) 755–762.

[7] F. Agostini, F. Skoczylas, Z. Lafhaj, About a possible valorisation in cementitious materials of polluted sediments after treatment, Cem. Concr. Compos. 29 (4) (2007) 270–278.

[8] A. Bentur, S. Igarashi, K. Kovler, Prevention of autogenous shrinkage in high-strength concrete by internal curing using wet lightweight aggregates, Cem. Concr. Res. 31 (11) (2001) 1587–1591.

[9] S. Weber, H.W. Reinhardt, A new generation of high performance concrete: concrete with autogenous curing, Adv. Cem. Based Mater. 6 (2) (August 1997) 59–68.

[10] RILEM TC-196, in: K. Kovler, O.M. Jensen (Eds.), Internal curing of concrete, state-of-the-art report of RILEM technical committee 196-ICC, RILEM Publications S.A.R. L., France, Bagneux, 2007, 139 pp.

[11] A.M. Neville, Properties of Concrete, 4th ed.Longman Publishing, London, 1996.

[12] H. Al-Khaiat, M.N. Haque, Effect of initial curing on early strength and physical properties of a lightweight concrete, Cem. Concr. Res. 28 (6) (1998) 859–866.

[13] I.A. Chen, M.C.G. Juenger, Incorporation of waste materials into Portland cement clinker synthetized from reagent-grade chemicals, Int. J. Appl. Ceram. Technol. 6 (2) (2009) 270–278.

[14] F. Andreola, L. Barbieri, I. Lancellotti, M.C. Bignozzi, F. Sandrolini, New blended cement from polishing and glazing ceramic sludge, Int. J. Appl. Ceram. Technol. (2009) 1–10 (to appear).

[15] H. Alanyali, M. Çöl, M. Yilmaz, S. Karagöz, Concrete produced by steel-making slag (basic oxygen furnace) addition in Portland cement, Int. J. Appl. Ceram. Technol. (2008) 1–13 (to appear).

[16] D.P. Bentz, K.A. Snyder, Protected paste volume in concrete: extension to internal curing using saturated lightweight fine aggregate, Cem. Concr. Res. 29 (11) (November 1999) 1863–1867.

[17] D. Cusson, T. Hoogeveen, Internal curing of high-performance concrete with pre-soaked fine lightweight aggregate for prevention of autogenous shrinkage cracking, Cem. Concr. Res. 38 (6) (June 2008) 757–765.

[18] S. Aroni, M. Polivka, Effect of Expanded Shale Aggregate on Properties of Expansive-Cement Concrete, in: J. Ujhelyi (Ed.), Proceedings of the RILEM Symposium On Testing and Design Methods of Lightweight Aggregate Concretes, 1967, RILEM, Budapest, Hungary.

[19] M. Barra de Oliveira, E. Vasquez, The influence of retained moisture in aggregates from recycling on the properties of new hardened concrete, Waste Manage. 16 (1–3) (1996) 113–117.

[20] C.S. Poon, Z.H. Shui, L. Lam, H. Fok, S.C. Kou, Influence of moisture states of natural and recycled aggregates on the slump and compressive strength of concrete, Cem. Concr. Res. 34 (2004) 31–36.

[21] K.K. Sagoe-Crentsil, T. Brown, A.H. Taylor, Performance of concrete made with commercially produced coarse recycled concrete aggregate, Cem. Concr. Res. 31 (5) (2001) 707–712.

[22] R. Wasserman, A. Bentur, Interfacial interactions in lightweight aggregate concretes and their influence on the concrete strength, Cem. Concr. Compos. 18 (1996) 67–76.

[23] K.L. Scrivener, A.K. Crumbie, P. Laugesen, The Interfacial Transition Zone (ITZ) between cement paste and aggregate in concrete, Interface Sci. 12 (2004) 411–421.

[24] J.A. Larbi, Microstructure of the interfacial zone around aggregate particles in concrete, Heron 38 (1) (1993) 1–69.

[25] T.Y. Lo, H.Z. Cui, Effect of porous lightweight aggregate on strength of concrete, Mater. Lett. 58 (6) (February 2004) 916–919.

[26] T.Y. Lo, H.Z. Cui, Spectrum analysis of the interfacial zone of lightweight aggregate concrete, Mater. Lett. 58 (2004) 3089–3095.

[27] A. Elsharief, M.D. Cohen, J. Olek, Influence of lightweight aggregate on the microstructure and durability of mortar, Cem. Concr. Res. 35 (2005) 1368–1376.

[28] Y. Benachour, C.A. Davy, F. Skoczylas, H. Houari, Effect of a high calcite filler addition upon microstructural, mechanical, shrinkage and transport properties of a mortar, Cem. Concr. Res. 38 (2008) 727–736.

[29] H. Moosberg-Bustnes, B. Lagerblad, E. Forssberg, The function of fillers in concrete, Mater. Struct. 37 (2004) 74–81.

[30] K.L. Scrivener, K.M. Nemati, The percolation of pore space in the cement paste/aggregate interfacial zone of concrete, Cem. Concr. Res. 26 (1) (1996) 35–40.

[31] F. Agostini, Inertage et valorisation des sédiments de dragage marins, PhD thesis (in French), Université des Sciences et Technologies de Lille/Ecole Centrale de Lille, 2006.

[32] F. Barberon, V. Baroghel-Bouny, H. Zanni, B. Bresson, J.B. d'Espinose de la Caillerie, L. Malosse, Z. Gan, Interactions between chloride and cement-paste materials, Magn. Reson. Imaging 23 (2005) 267–272.

[33] F. Agostini, F. Skoczylas, Z. Lafhaj, Behaviour of Mortar Incorporating Polluted Harbour Sediments after Treatment, Proceedings of the First Euromediterranean Symposium on advances in Geomaterials and Structures, Hammamet, Tunisia, May 2006, pp. 173–178.

[34] P.Y. Scordia, Caractérisation et valorisation de sédiments fluviaux pollués et traités dans les matériaux routiers, PhD thesis (in French), Université des Sciences et Technologies de Lille/Ecole Centrale de Lille, 2008.

[35] French and European Standard NF EN-12350-2, Essai pour béton frais—partie 2: essais d'affaissement (Testing fresh concrete-Part 2: slump test), 1999.

[36] R. Zaharieva, F. Buyle-Bodin, F. Skoczylas, E. Wirquin, Assessment of the surface permeation properties of recycled aggregate concrete, Cem. Concr. Compos. 25 (2003) 223–232.

[37] Y. Benachour, C.A. Davy, F. Skoczylas, H. Houari, Effect of a high calcite filler addition upon microstructure and freeze/thawing resistance of a mortar, in: Proceedings of the International Conference CONCREEP 2008 on Creep, Shrinkage and Durability Mechanics of Concrete and Concrete Structures, Kashikojima Island, Ise-Shima, Japan, CRC Press, Taylor and Francis Group, Balkema Ed., 2008, pp. 993–998.

[38] P. Mounanga, Etude expérimentale du comportement de pâtes de ciment au très jeune âge : hydratation, retraits, propriétés thermophysiques, PhD thesis (in French), Université de Nantes/Faculté des Sciences et Technologies, France, 2003.

[39] H.F.W. Taylor, Cement Chemistry, 2nd editionTelford Publishing, London, 1997.

[40] I.G. Richardson, The nature of C–S–H in hardened cements, Cem. Concr. Res. 29 (1999) 1131–1147.

[41] K.S. Chia, M.-H. Zhang, Water permeability and chloride penetrability of high strength lightweight aggregate concrete, Cem. Concr. Res. 32 (4) (April 2002) 639–645.

[42] K.O. Kjellsen, A. Monsoy, K. Isachsen, R.J. Detwiler, Preparation of flat-polished specimens for SEM-backscattered electron imaging and X-ray microanalysis—importance of epoxy impregnation, Cem. Concr. Res. 33 (2003) 611–616.